ACCSCIENCE PUBLISHING

Materials Science in Additive Manufacturing

ORIGINAL RESEARCH ARTICLE

Energy absorption and recoverability of Moore space-filling thin-walled structures

Changlang Wu, Vuong Nguyen-Van, and Phuong Tran*

School of Engineering, RMIT University, Melbourne, VIC 3000, Australia

Abstract

This paper proposes novel thin-walled structures inspired by Moore space-filling curves. Nine designs, featuring three fractal hierarchies (1st, 2nd, and 3rd orders) with three different relative densities (20%, 30%, and 40%), were used as cross-sectional configurations of the thin-walled structures. Specimens were manufactured using a material extrusion additive manufacturing technique, fused filament fabrication, with a carbon fiber-reinforced composite. Quasi-static compression tests from in-plane direction were conducted to investigate the influences of fractal hierarchy and relative density on the energy absorption capacity. Finite element models were developed to compare with the experiments and to further explore the 4th order structures. A certain level of compliance and snap-in instability were observed in all the structures. These properties show great potential for such thin-walled structures to absorb more energy by enduring large strain. Among them, the 2nd order structures exhibited the best energy absorption capacity. Furthermore, loading and unloading compression tests were performed on the 2nd and 3rd order structures (relative density of 20%) to evaluate their resilience toward displacement and damages. The residual strain and dissipated energy ratio demonstrated that the 2nd order structure outperformed the 3rd order structure owing to its less compliant feature. The integration of Moore curves with thin-walled structures contributes to great compliance and snap-in instability, offering a new approach to designing lightweight energy absorption structures.

Keywords: Fractal; Compliant structures; Snap-in instability; Energy absorption; Additive manufacturing

***Corresponding author:**
Phuong Tran
(jonathan.tran@rmit.edu.au)

Citation: Wu C, Nguyen-Van V, Tran P, 2023, Energy absorption and recoverability of Moore space-filling thin-walled structures. *Mater Sci Add Manuf,* 2(1): 53.
https://doi.org/10.36922/msam.53

Received: February 20, 2023

Accepted: March 7, 2023

Published Online: March 24, 2023

1. Introduction

Energy absorption has always been one of the design objectives to provide protection to humans and structures during dynamic or impact events, such as high specific energy absorption (SEA)[1-4], lightweight[5-8], low cost[5,9,10], and easy installation[11,12]. Among various types of structures, thin-walled structures have been widely used as effective energy absorbers in civil engineering, automobile engineering, aerospace engineering, etc., considering its excellent energy absorbing capacity and lightweight features[13]. Over the past decades, designing lightweight thin-walled structures without sacrificing their energy absorption or crashworthiness has become a hot research topic. It has been demonstrated that the energy absorption capacity of thin-walled structures is influenced by various factors, such as structural configuration, material selection, and trigger

arrangement. Among them, the cross-section profile is one of the most critical factors[13]. Various shapes have been explored for the outer layer tubes, including triangle[14,15], square[16-18], pentagon[19], hexagon[20], and circle[14,15,21,22] and more recently different cross-section designs for the infill have been proposed and elaborated[23-25].

When it comes to cross-sectional configurations, nature-inspired patterns are often employed due to its multi-functional features and outperformed characteristics[26,27]. One of the fascinating patterns that could be found in nature is the fractal, for instance, the galaxy and seashell. Fractal, as defined in mathematics, is a geometry that resembles itself at various scales[28]. Several studies investigating the crashworthiness of fractal-inspired thin-walled structures (Figure 1) have provided a new approach to designing novel lightweight energy absorbers with improved crashing characteristics[29-32]. In 2018, Zhang *et al.*[23] investigated the crashworthiness of fractal hierarchical hexagon thin-walled structures that were inspired by spider webs. Fractal configurations, geometrical parameters, and fractal orders have proven to play important roles in energy absorption. Besides, Wang *et al.*[24] proposed a thin-walled structure design with cross-sections of Koch snowflakes. Interestingly, the 2nd order Koch snowflake design outperformed a wide range of multi-cell structures with the same mass, thus supporting the argument proposed by Zhang *et al.*[23]. Numerically and analytically, Huang *et al.*[26] introduced a gradient fractal thin-walled structure inspired by bamboos to improve the SEA, comparing to conventional square honeycombs. Again, the 2nd order fractal tube yielded the best energy absorption per unit mass.

To improve the energy absorption capacity of fractal-inspired thin-walled structures, reinforcements have been used as infills. In early 2000, hollow foam-filled tubes were studied analytically and numerically to demonstrate the higher weight-efficiency in energy absorption[33]. Compared to tubes without foam-infill, hollow foam-filled tubes exhibited higher energy absorption capacity with the same mass. Similarly, Dadrasi *et al.*[34] conducted a study to compare the crashworthiness of another fractal-pattern inspired thin-walled columns with and without foam-infill.

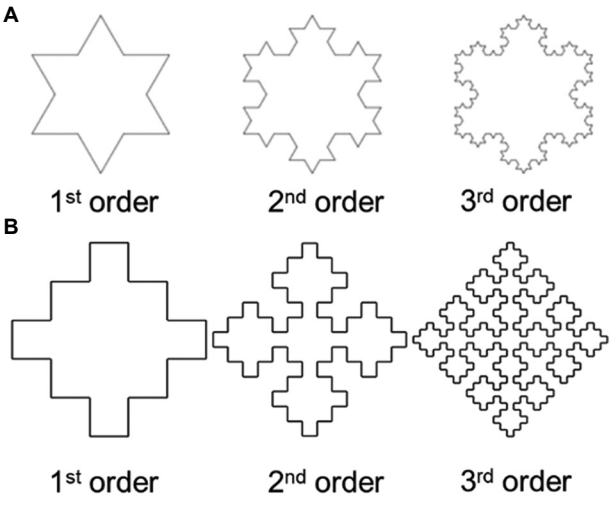

Figure 1. Fractal cross-sections employed in thin-walled structure design: (A) Koch snowflake; (B) Sierpiński curve.

The previous studies have focused on the out-of-plane crashworthiness of structures as vertical thin-walls are known to provide strength and stiffness. Moreover, most of the structures have integrated fractal patterns with a thin-walled tube as the outer layer to improve their mechanical properties. However, this outer layer tube adds extra weight and cost.

Furthermore, fatigue damage also plays an important role in energy absorption[35,36]; therefore, cyclic performance is critical for energy absorption in engineering applications[37]. An energy absorbing device with low recoverability after cyclic loading is likely to have a short lifespan, which could potentially lead to casualties, structural damages, and extra maintenance cost. However, loading and unloading cyclic compression experiments have not been studied on any fractal-inspired thin-walled structures. Moore space-filling curves, as another type of fractal structure, are rarely used as the design motif for thin-walled structures. Space-filling curves are characterized by a unique feature, that is, a finite area would be filled with a curve of infinite length after an infinite number of iterations. Theoretically, Moore space-filling curves could fill a limited design space with infinite length of curves. For a given relative density of thin-walled structures, the cross-section could be filled with infinite space-filling curves by increasing fractal hierarchy. Thus, thin-walled structures with such cross-sectional configurations could offer great potential for excellent mechanical responses in the in-plane direction[38].

From the design point of view, many studies have been carried out over the past few decades on different cross-sectional shapes of thin-walled structures. However, the complex geometries of cross-sectional configurations have yet to be explored due to the limitations of conventional manufacturing technology[39]. The manufacturing process of structures with complex geometries has become easier than ever using advanced additive manufacturing (3D printing) techniques[40-42]. The main purpose of the present work was to study energy absorption for a novel compliant thin-walled structure. These newly designed infill patterns were inspired from Moore space-filling curves with three fractal hierarchies. Three relative densities, that is, 20%, 30%, and 40%, were investigated for each

design. All the specimens were manufactured using fused filament fabrication (FFF), which is a low-cost additive manufacturing technology. Quasi-static compression tests and loading-unloading cyclic compression tests were also carried out to observe the mechanical responses and evaluate the permanent deformation of the proposed structures. Numerical models were developed and used for a parametric study to further analyze the mechanical behaviors.

2. Methodology

2.1. Design and fabrication of compliant structures

The novel metamaterials were inspired from a series of space-filling infill patterns, known as Moore curves. As illustrated in Figure 2A, this set of curves consisted of many orders. The 0th order was constructed by connecting the centers of each small square from the bottom left to the bottom right. The 1st order comprised four of the 0th order in a smaller scale with certain rotations. By repeating the same procedure, the 2nd and 3rd order curves were derived (Figure 2A). By connecting the opening with a straight line and smoothing the corner using cubic spline function, the cross-section centerline was constructed. All the curvatures at the same locations were constant for all designs; the only design parameter was wall thickness. The structures were constructed by assigning certain thickness to the wall and extrusion along the out-of-plane direction.

The first three orders of Moore curves were adopted to investigate the influence of fractal hierarchy on energy absorption capacity. In addition, three different relative densities were applied, that is, 20%, 30%, and 40%, to explore the effect of relative density on mechanical responses. All the proposed designs had a depth of 15 mm (in-plane depth) and a side length of 50 mm. In other words, the block size (width × length × height) was 50 × 50 × 15 mm. To achieve three relative densities, the wall thickness was adjusted accordingly, as shown in Table 1.

The samples were fabricated with a composite material, onyx, using an FFF printer, MarkTwo (Markforged Inc., USA). The onyx, provided by Markforged, was composed of nylon (80 vol%) and short carbon fibers (20 vol%). The carbon fibers were 200 μm in length and orientated in the printing direction[43]. An extruder of 0.4 mm in diameter was used for filament deposition. The printing parameters were the same for all specimens: 0.1 mm layer height, single-layer outline, and solid infill with a −45°/45° pattern. For each layer, the extruder travelled along the outlines of the structure first and filled the space in between the outlines. Therefore, the thinnest wall thickness that could be fabricated using Markforged was 0.8 mm (twice of the resolution). Based on this principle, the smallest relative density of 20% was adopted to ensure the printing quality. In addition, the limitation of wall thickness restricted the fractal hierarchy up to the 3rd order. The 3D-printed thin-walled structures with a relative density of 20%, 30%, and 40% are presented in Figure 2B-D, respectively.

The thickness of the fabricated specimens was measured from several regions of the cross-sections to compare to the design values (Table 1). Overall, the 3D-printed structures were slightly thicker than the original designs. One reason could be the high extrusion flow rate, resulting in over-extrusion of filament and a thicker print line. Within each specimen, the wall thickness was not consistent due to machine inaccuracy from FFF printing. As an important printing parameter, the pressure in the extruder influences the filament thickness during the

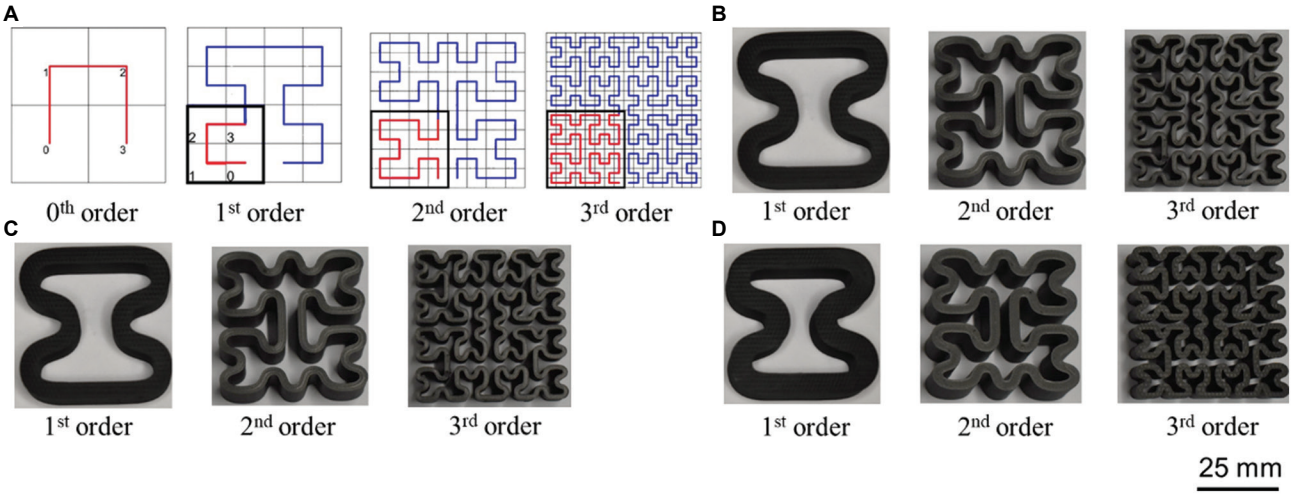

Figure 2. (A) First three hierarchies of theoretical Moore curves. Manufactured Moore curve-inspired thin-walled structures with a relative density of (B) 20%, (C) 30%, and (D) 40%.

Table 1. Wall thickness comparison between designs and as-fabricated specimens

Wall thickness (mm)	1st order		2nd order		3rd order	
	Designed	Fabricated	Designed	Fabricated	Designed	Fabricated
rd=20%	3.110	3.17–3.27	1.610	1.60–1.83	0.840	0.85–0.89
rd=30%	4.665	4.66–4.88	2.415	2.58–2.67	1.260	1.35–1.42
rd=40%	6.220	6.16–6.32	3.220	3.22–3.43	1.680	1.75–1.93

rd: Relative density. Measurements of fabricated specimens were made using a caliper with precision of two decimal places

printing process of each layer. The extruder is expected to generate a filament line with uniform width. However, a thin print line in the beginning may widen as the nozzle pressure increases. This could be more distinct when printing curves, which is a characteristic feature in Moore curve-inspired structures.

2.2. Quasi-static and cyclic compression tests

Uniaxial compression tests were performed using Instron's universal testing machine (5900R Series), with a 30 kN load cell. A loading rate of 2 mm/min was applied to all testings. Unit cells were compressed up to 70% strain (displacement of 35 mm) from two in-plane directions. Three specimens were tested for each design to ensure the reliability of results. Force-displacement data and real-time videos were captured and recorded from the experiment to study the responses of different structures. To further investigate the energy absorption performance of the metamaterials, loading and unloading compression tests were conducted. Herein, cyclic experiments were adopted to obtain the structural response of low cyclic-loading events, such as earthquake[44]; however, fatigue was not considered. Six cycles were applied to each specimen. Force-displacement curves were captured to estimate energy absorption and then converted to effective stress-strain curves to evaluate the residual strain.

SEA, which is defined as the amount of energy absorbed by the material per unit mass, has been widely used as a parameter to indicate the energy absorption capacity of a crushed material[45]. SEA can be calculated by integrating the force-displacement curve (Figure 3A) and then divided by the total mass of materials[43]:

$$SEA = \int_0^d \frac{F(x)}{m} \mathrm{d}x, \tag{I}$$

Where F (x) is the reaction force captured by load cell during experiment, x denotes the compression displacement, and m is the mass of the structure.

To compare the performance of different designs, effective stress-strain curves were derived from force-displacement curves and compared. The following equations were used to calculate the effective axial stress (σ^*_{yx}) and effective axial strain (ε^*_{yx}) in the y-direction (compression direction):

$$\sigma^*_{yx} = \frac{R_y}{A_y}, \tag{II}$$

$$\varepsilon^*_{yx} = \frac{\delta_y}{L_y} \tag{III}$$

Where R_y is the total reaction force from the structure, while A_y is the cross-sectional area of the whole structure that is perpendicular to the y-direction; L_y denotes the height of the structure (length along y-direction), while δ_y is the total displacement experienced by the structures along the y-direction.

For cyclic testings, two parameters were used to evaluate the performance of the structures. First, residual strain was measured after the first and all six loading-unloading cycles to assess the amount of plastic deformation. Second, dissipated energy, which is referred as plastic strain energy, was calculated by subtracting the released energy during the reloading period from the stored energy during the loading period (Figure 3B)[46].

Based on the definition of dissipated energy ($E_{dissipated}$), it was calculated from the force-displacement curve accordingly:

$$E_{stored} = \int_0^{x^n_{max}} F(x)^n_{loading}\, dx \tag{IV}$$

$$E_{released} = \int_0^{x^n_{max}} F(x)^n_{unloading}\, dx, \tag{V}$$

$$E_{dissipated} = E_{stored} - E_{released}, \tag{VI}$$

Where E_{stored} is the sum of energy stored in the structure during all loading cycles, $E_{released}$ is the sum of energy released from the structure during all unloading cycles, and n is the total number of loading and unloading cycles.

To evaluate the resilience of the proposed structures toward permanent deformation and potential damage

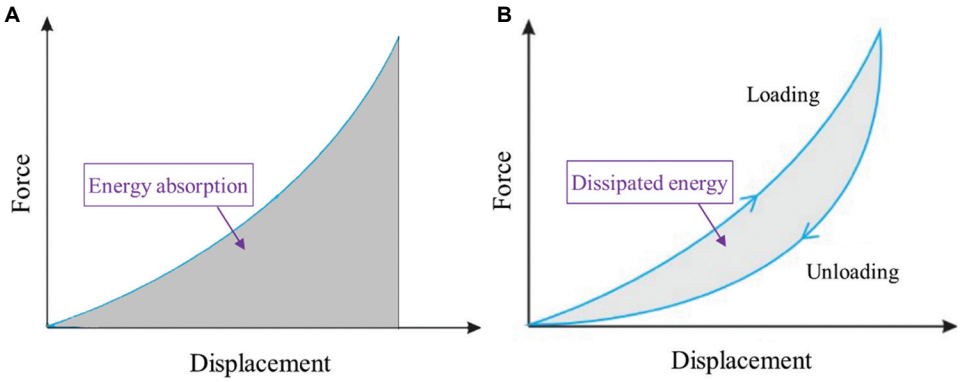

Figure 3. (A) Energy absorbed by the structure represented by the area under force-displacement curve. (B) Energy dissipated by the structure represented by the area between the loading and unloading force-displacement curve.

caused by cyclic loading, we used an energy dissipation ratio (η), which is defined as the ratio between total dissipated energy and total stored energy:

$$\eta = \frac{E_{dissipated}}{E_{stored}} \quad \text{(VII)}$$

2.3. Numerical models and convergence study

A 3D nonlinear quasi-static finite element (FE) model was developed to simulate the response of the structures under compression loading using the commercial software package Abaqus/Explicit 2020 (Dassault Systems SIMULIA Corp., Providence, RI). The material properties used in the model were obtained from the tensile tests on 3D-printed onyx specimens under ASTM D638, rendering a Young's modulus value of 1,800 MPa and a yield stress of 61 MPa. Adopted from the onyx datasheet provided by Markforged, the density and Poisson's ratio were 1.2 g/cm^3 and 0.3, respectively.

To reduce the computational cost and maintain large-scale simulation, the model was simplified by using shell elements considering a constant wall thickness. The linear four-node shell elements (S4R) were used to simulate the fractal structures. Considering that the metallic compression plates of Instron's universal testing machine were much stiffer than the 3D-printed Onyx samples, two rigid plates were modeled for simplification. The shell elements were defined to have a normal contact behavior using hard contact formulation, while a friction coefficient of 0.3[47] was utilized to describe the tangential responses. Two reference points were created, with rigid body constraints applied between them and the rigid plates. By controlling the boundary conditions on the two reference points, the uniaxial compression test conditions were simulated (Figure 4). A displacement of 35 mm was applied at the top reference point, while an all-direction fixed boundary condition was assigned to the bottom reference point.

Besides, the optimal mesh size was decided after carrying out convergence study on the 2nd order fractal structure (relative density of 20%) loaded from both directions. Mesh sizes of 0.5 mm, 0.75 mm, 1.5 mm, and 3 mm were applied for the shell elements. Results of the reaction force versus displacement curves obtained from simulations are shown in Figure 4C and D, corresponding to loading direction 1 (LD1) and loading direction 2 (LD2), respectively. It could be inferred that the mesh size of 0.75 mm is the optimal considering the model accuracy and computational cost.

Furthermore, a parametric study on 4th order fractal-inspired thin-walled structures was conducted using FE simulations. Limited by Markforged printer's resolution, 4th order structures with relative densities of 20%, 30%, and 40% could not be manufactured. Using the FE model, the energy absorption of higher-order fractal-inspired structures was studied.

3. Results and discussion

3.1. Effective stress-strain curves

3.1.1. Quasi-static compression test results

The quasi-static compression test of the 2nd order fractal sample is illustrated in Figure 5D. The responses of the metamaterials under quasi-static compressive load from in-plane direction 1 are shown in Figure 5A-C, corresponding to three different relative densities (20%, 30%, and 40%, respectively). Curves were constructed using the mean effective stress value from three testing results. Overall, all the structures underwent large strains with very low stress. Excellent compliance was observed up to around 50% strain. As suggested in Figure 5A-C, the 3rd order thin-walled structures with a relative density of 20% yielded the most compliant behavior.

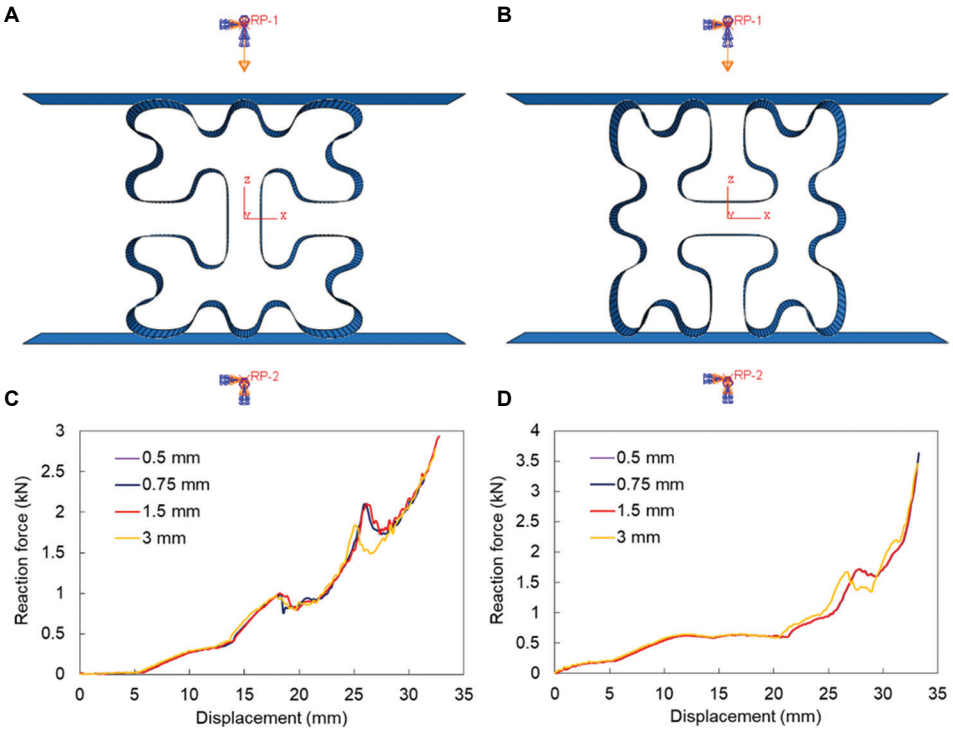

Figure 4. Boundary conditions on reference points to simulate 2nd order fractal structures with shell elements from (A) loading direction 1 (LD1) and (B) loading direction 2 (LD2). Mesh size convergence study on the 2nd order (20% relative density) structure from (C) LD1 and (D) LD2.

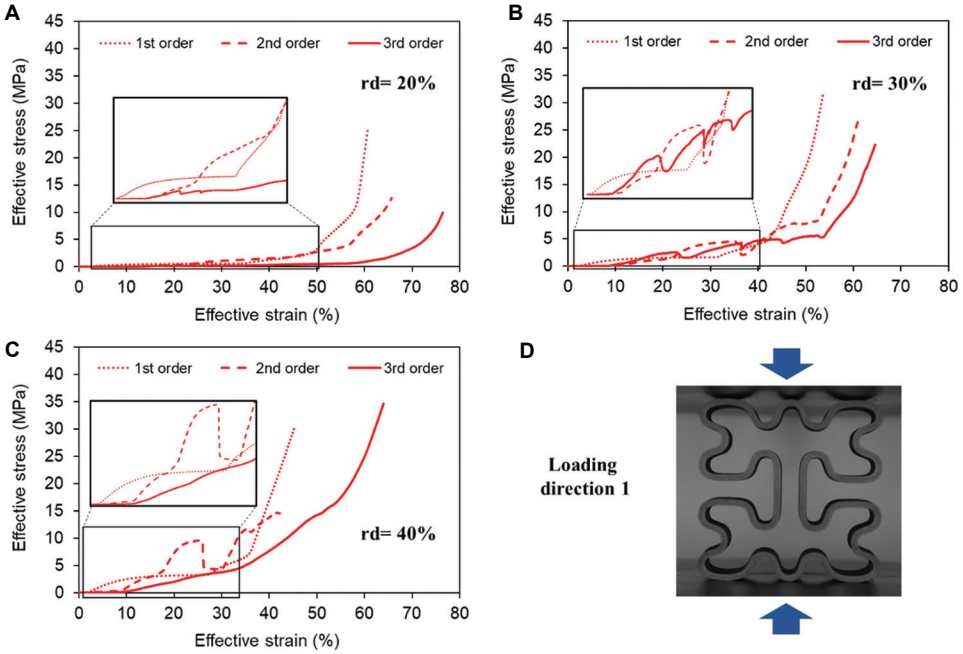

Figure 5. Effective stress-strain curves obtained from quasi-static compression test from loading direction 1 (LD1): (A) Relative density (rd) = 20%, (B) rd = 30%, and (C) rd = 40%. (D) 2nd order structure being compressed from LD1. Magnified images in A–C provide clearer views for comparing the beginning responses during compression.

Another characteristic feature of all the effective stress-strain curves was the jagged pattern, which suggested numerous sudden stress drops from the snap within the structures during compression. The snaping was attributed

to the nature of space-filling curves and the smooth-corner design. When being compressed, some parts of the structure collided with other parts. Since Moore space-filling curves meander within a limited space, the concave and the adjacent convex tend to snap into each other. Due to snap-in instability, stress within the structure redistributes and decreases. Instead of densification, these fractal structures utilize their compliance to endure more strain before failure.

When applying load from in-plane direction 2, the structures behaved in a different way compared to LD1 (Figure 5). Effective stress-strain curves for three different relative densities are shown in Figure 6. Similar to responses from LD1, structures with 20% relative density experienced larger strain under the same effective stress compared to those with a higher relative density. For the same relative density, the 3rd order structures demonstrated the most compliant behavior. Comparing to the responses from LD1, the stress-strain curves were more jagged. This could be explained by more curvature changes of the cross-section in vertical direction when compressed from LD2. The snap-in behavior was prominent especially for the 1st order structure, followed by the 2nd and 3rd order structures. While the drops in the effective stress-strain curves for the 2nd and 3rd order structures became smaller, the number of total drops increased due to the nature of space-filling curves.

Among all the curves, the response from LD2 for the 3rd order structure with 30% relative density was the most jagged. To understand the reasons behind these stress drops in all the stress-strain curves, the behaviors of the 3rd order structure (30% relative density) observed from the experiment are presented in Figure 7. Structural deformations at strains of 15%, 20%, 25%, 30%, 35%, 40%, and 45% are displayed to provide a clearer picture of the dramatic stress drops at points A, B, and C (highlighted in the stress-strain curve). From the original configuration to a strain of 15%, the thin-walled structure contracted in a perpendicular direction due to the gaps in the space curve. Thereafter, there was contact within the structure itself, as shown in the deformation at a strain of 20%. Collisions within the structure led to one convex part snapping-in to an adjacent concave part, which could be found in the magnified images in Figure 7.

For instance, at a strain of 25%, the two convex parts, as shown in the solid green square in Figure 7, were confronting each other. With increasing load, the top convex slipped all the way into the concave gap on its bottom right (green dashed square in Figure 7 at a strain of 30%). The sudden snap-in was an instability created by the features of Moore curves and the smooth-corner design of the thin-walled structures. Stress was redistributed due to the snap-in behavior within a short time, leading to stress drop A (stress-strain curve in Figure 7). A similar phenomenon

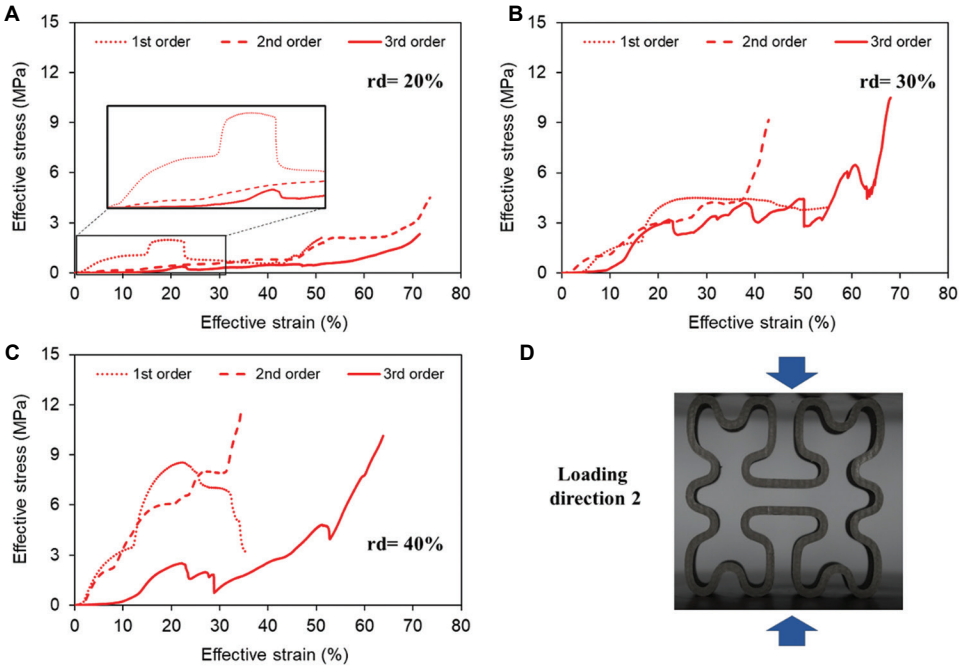

Figure 6. Effective stress-strain curves obtained from quasi-static compression test from loading direction 2 (LD2): (A) Relative density (rd) = 20%, (B) rd = 30%, and (C) rd = 40%. (D) 2nd order structure being compressed from LD2. The magnified image in A provides a clearer view for comparing the beginning responses during compression.

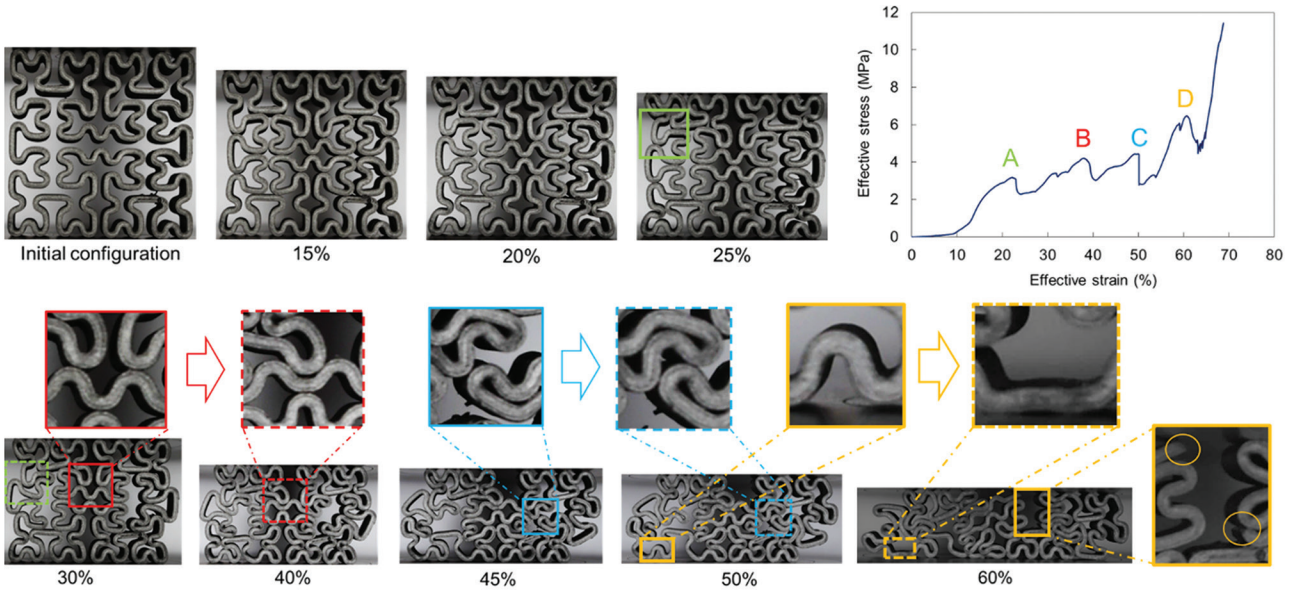

Figure 7. Configurations of 3rd order structure (relative density of 30%) during compression at different strains. Squares colored green, red, and blue show the deformation change of the structure causing stress drops A, B, C, and D, respectively, as highlighted in the stress-strain curve. Magnified images showing the snap-in behaviors, straightening of curved elements, and failure within the structure.

was observed at compression strains of 40% and 50%, corresponding to stress drops B and C, respectively. The basis of the descend after local peak D was the straightening of curved elements and damages within the structure (see yellow magnified images in Figure 7). Compared with the 1st and the 2nd order structures, the 3rd order structure showed a more complex cross-sectional geometry with more concave/convex. Hence, the response of the 3rd order structure demonstrated more drops in stress.

3.1.2. Cyclic loading test results

As observed from the results of the quasi-static compression tests, the 2nd and 3rd order metamaterials with relative density of 20% revealed their characteristic compliance feature. Hence, a cyclic compression test with six loading-unloading cycles was performed to further investigate the energy absorption performance of fractal-inspired thin-walled structures. Figure 8 shows the effective stress-stain curves for both 2nd and 3rd order structures under cyclic loading from direction 1 and 2. Overall, for each design, the response of the first cycle was different from the following five cycles. The structure behaved in a similar way during the last five cycles regardless of the loading direction, demonstrating the reliability and recoverability of the structures to some extent. In other words, most of the plastic deformation during the whole cyclic loading test occurred in the first cycle[48].

Besides, the 2nd order structure appeared to have higher recoverability after cyclic loading than the 3rd order structure through a comparison of their post-mortem deformations (Figure 8). The deformed shapes of the specimens before and after cyclic loading are illustrated in Figure 8. The 2nd order structure maintained its original shape with a certain degree of contraction, while the 3rd order structure experienced significant permanent deformation.

3.2. FE model validation

The FE simulation results were validated by comparing to the experimental outcomes in terms of the effective stress-strain curves of the fractal structures with a relative density of 20% (Figure 9). The behaviors from numerical simulation were close to what was observed from the experiment. However, there were still some discrepancies. Figure 9 presents the effective stress-strain curves from the experiments and simulations. In general, the strain and stress predicted from numerical models were higher than those captured in experiments. In the simulation, there was no obvious sliding between rigid plates and fractal structures. Nevertheless, the top and bottom of the fractal structures that were in contact with the metal compression plates slipped along the tangential direction. Despite applying a frictional penalty of 0.3 to the tangential interaction between surfaces in the FE model, the coefficient of friction between the metal plates and the fractal structures during experiment seemed to be smaller. The sliding attributed to the lower strain and stress in the experiment compared to the simulation.

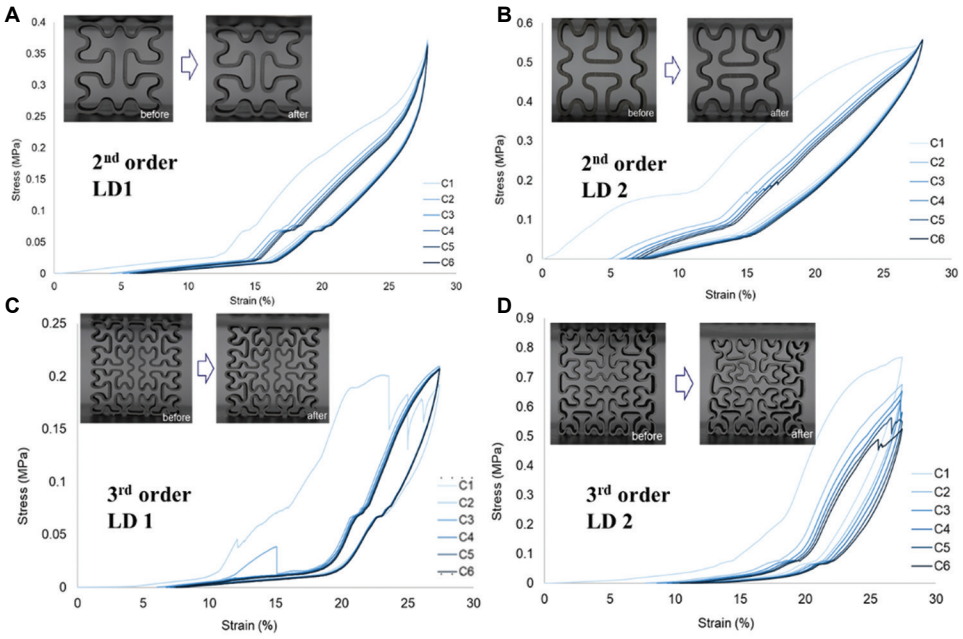

Figure 8. Effective stress- strain curves obtained from cyclic compression tests for structures with a relative density of 20%: (A) 2nd order from loading direction 1 (LD1), (B) 2nd order from loading direction 2 (LD2), (C) 3rd order from LD1, and (D) 3rd order from LD2. The pictures of the specimens are the configurations before and after the cyclic tests.

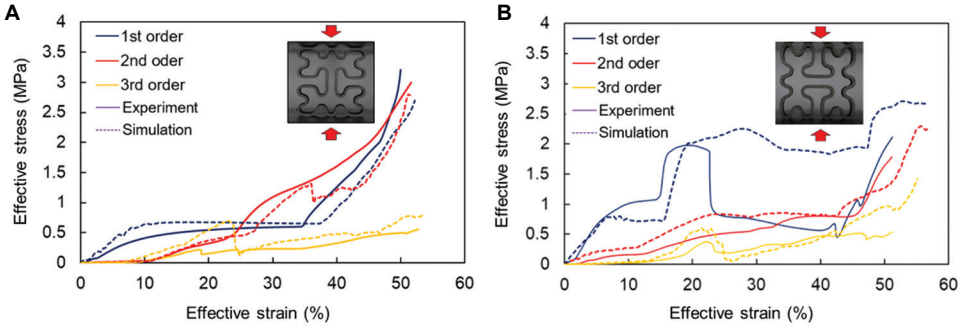

Figure 9. Comparisons of effective stress-strain curves obtained from quasi-static compression experiments and FE simulations for 2nd order fractal structure with a relative density of 20% from (A) loading direction 1 and (B) loading direction 2.

As displayed in Figure 9B, the effective stress (Equation II) within the 1st order structure in the experiment dropped drastically at a strain of 22%. However, there was no obvious reduction in stress, but rather a long phase of plateau from the numerical simulation. In other words, no snap-in was observed in the FE modeling. This is ascribed to the perfectly symmetric parts and ideal boundary conditions in the numerical model. Meanwhile, the experimental condition and 3D-printed specimens differed from what was established in the modeling. It is widely known that defects commonly exist in FFF technology using carbon fiber-reinforced polymer[49]. Any misalignment of compressive loading or imperfections within the fabricated structures could give the structures opportunity to behave in an asymmetric way, leading to the snap-in phenomenon.

When comparing the response from LD1 to LD2, the difference between the experiment and the simulation was slightly smaller. This phenomenon is a result of the design of structures. As shown in Figure 4A and B, the total contact surface between the compression plates and specimens was larger in LD1 (Figure 4A). All the specimens deformed symmetrically in the FE models considering the symmetric design. During the experiment, structures with less contact surface were more prone to deform asymmetrically due to misaligned loading conditions or manufacturing defects.

3.3. Stress distributions

Failure of engineering components is mostly due to stress within the structure. The stress distribution reflects the level of structural design and affects the structural safety

performance[50]. It is important to measure and evaluate the stress distribution to ensure that the structure will maintain its integrity under a given load. Stress concentration, which indicates that the localized stress of a segment is significantly higher than the surrounding region, could cause structural failure even if the effective stress is smaller than the material yield strength. For a compliant structure, instability during compression is often accompanied by stress redistribution in a stress concentration region. Thus, it is important to study the stress distribution and observe the stress concentration regions in this study.

To better understand the behavior of structures captured in the experiment, simulations were performed with respect to various designs to observe the stress distribution within the structures. Figure 10 shows the deformation and equivalent stress distribution (von Mises stress) in the 2nd order structure (relative density of 20%) at strains of 25%, 35%, and 45%. In general, the stress was unevenly distributed at the cross-section of the fractal structure. While the concave segments (purple arrow in stress distribution at 25% strain in Figure 10) at the top and bottom were still experiencing very low stress, the four corners (yellow arrow in stress distribution at 25% strain in Figure 10) had already yielded. It is interesting to note that the fractal structures were inclined to act in an auxetic way[51]. With increasing compression load, the structures shrunk in a perpendicular direction rather than expanding. Similar responses were observed for all the fractal-inspired thin-walled structures.

Since the fractal design contains concaves and convexness, the corners with sudden change of curvature tend to induce more stress concentration than other regions. With the increase in strain, all the corners experienced very high stress except for the two corners in the middle due to the snap-ins from the adjacent structures, which attempted to expand the two middle corners and eventually led to curvature reduction. During this process, redistribution and reduction of stress occurred at these two locations. At a strain of 45%, there was accumulation of high stress at the bottom four corners (Figure 10) that were in contact with the compression plates, indicating densification.

3.4. SEA and energy dissipation

Based on the force-displacement curves directly obtained from Instron's machine, the SEAs for all nine designs were compared (Figure 11) with respect to different loading directions. SEA was calculated from 0% to 40% strains (before densification) for all structures. For both loading directions, the increase in fractal hierarchy led to less energy absorption for the relative density of 20%. With the increase in relative density, the energy absorption capacity significantly improved except for the 3rd order structure. In particular, the 2nd order structure appeared to be the most sensitive to relative density regardless of the loading direction. Specifically, the SEA for the 2nd order structure increased to more than double the amount with every 10% rise of relative density. It is interesting to note that for structures with 20% relative density, the 1st order exhibited the best energy absorption capacity among all three hierarchies. However, with increasing relative density, the efficiency of 2nd order structures in absorbing energy seemed to increase. When comparing LD1 with LD2, it could be observed that the energy absorption capacity was higher when subjected to LD2 than when subjected to LD1.

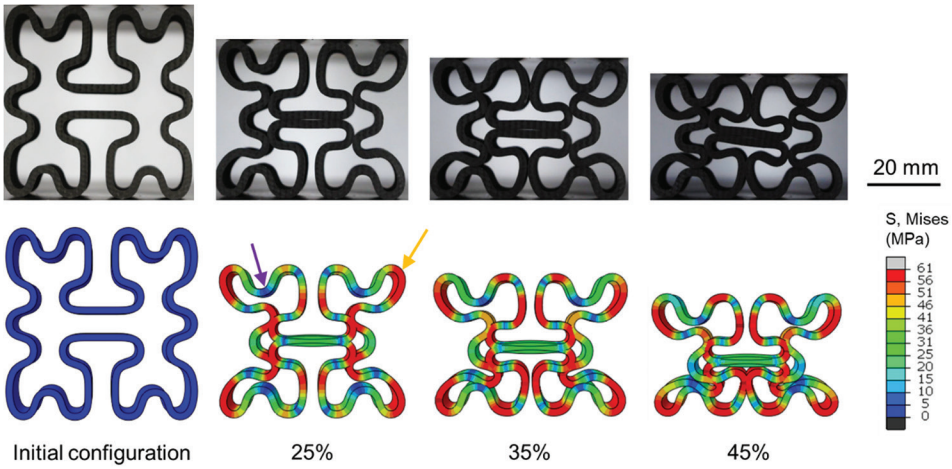

Figure 10. Deformation and stress distribution within the 2nd order structure (20% relative density) under compressive load from direction 2. The purple and yellow arrows refer to the typical concave and convex in the structural design. The configurations from the simulation are rendered with actual thickness.

To quantitatively evaluate the performance of fractal thin-walled structures during cyclic compression test, residual strain and dissipated energy (Equation VI) were calculated and compared in a bar chart (Figure 12). Recoverability was evaluated by the residual strain, which measures the permanent deformation of structures after a cyclic test. Dissipated energy, the strain energy dissipated in a material during cyclic loading, was calculated using stored energy during the loading period and the released energy during the unloading period. Both properties were measured after only the first cycle and after all six cycles, considering the difference in behavior during the first cycle and the remaining cycles. Overall, the energy dissipated within the first cycle was the highest among all six cycles. It could be inferred that both 2nd and 3rd order structures dissipated more energy under LD2 (Figure 12), considering the first cycle and all six cycles. Nevertheless, the residual strains in LD2 were higher than those in LD1. The dissipated energy and residual strain indicated that structures under load in direction 2 experienced more permanent deformation.

Table 2 compares the energy dissipation ratios (η) for both structures in two loading directions. The 2nd order structure had relatively smaller energy dissipation ratios than the 3rd order structure, while both structures were more efficient in LD1 (lower value of η). The residual

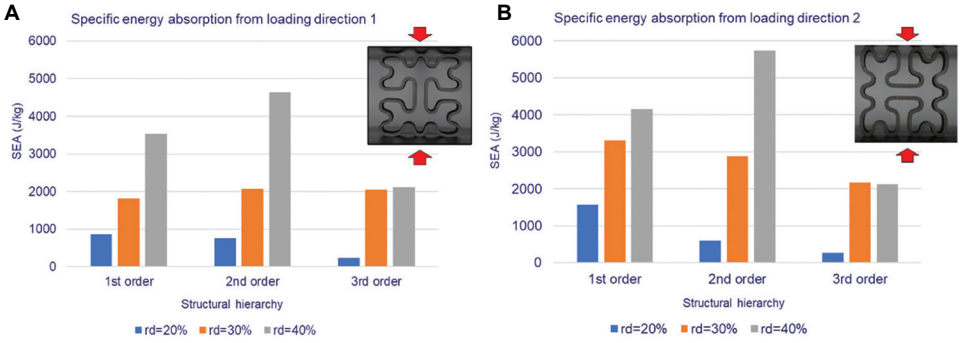

Figure 11. Specific energy absorption comparison among different hierarchies and various relative densities during quasi-static compression test from (A) loading direction 1 and (B) loading direction 2.
rd: Relative density.

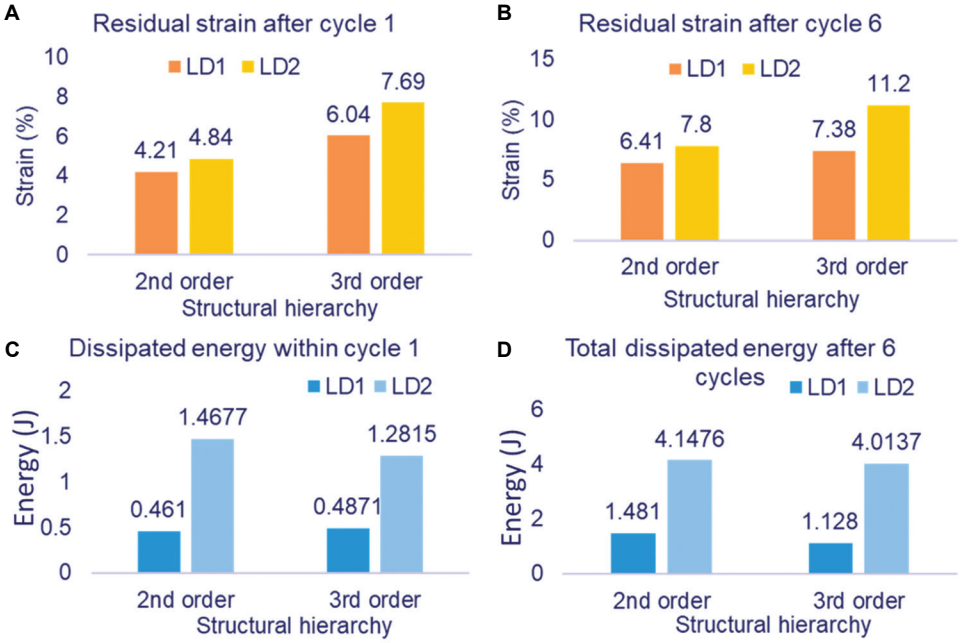

Figure 12. Comparisons for residual strain after (A) the first loading-unloading cycle and (B) all six loading-unloading cycles. Comparisons for dissipated energy after (C) the first loading-unloading cycle and (D) all six loading-unloading cycles.
LD1: Loading direction 1; LD2: Loading direction 2.

Table 2. Energy dissipation ratio for the 2nd and 3rd order structures after cyclic loading

Properties	2nd order structure		3rd order structure	
	Loading direction 1	Loading direction 2	Loading direction 1	Loading direction 2
Dissipated energy (J)	1.48	4.15	1.13	4.01
Stored energy (J)	4.57	11.11	2.64	7.82
Energy dissipation ratio	0.32	0.37	0.42	0.51

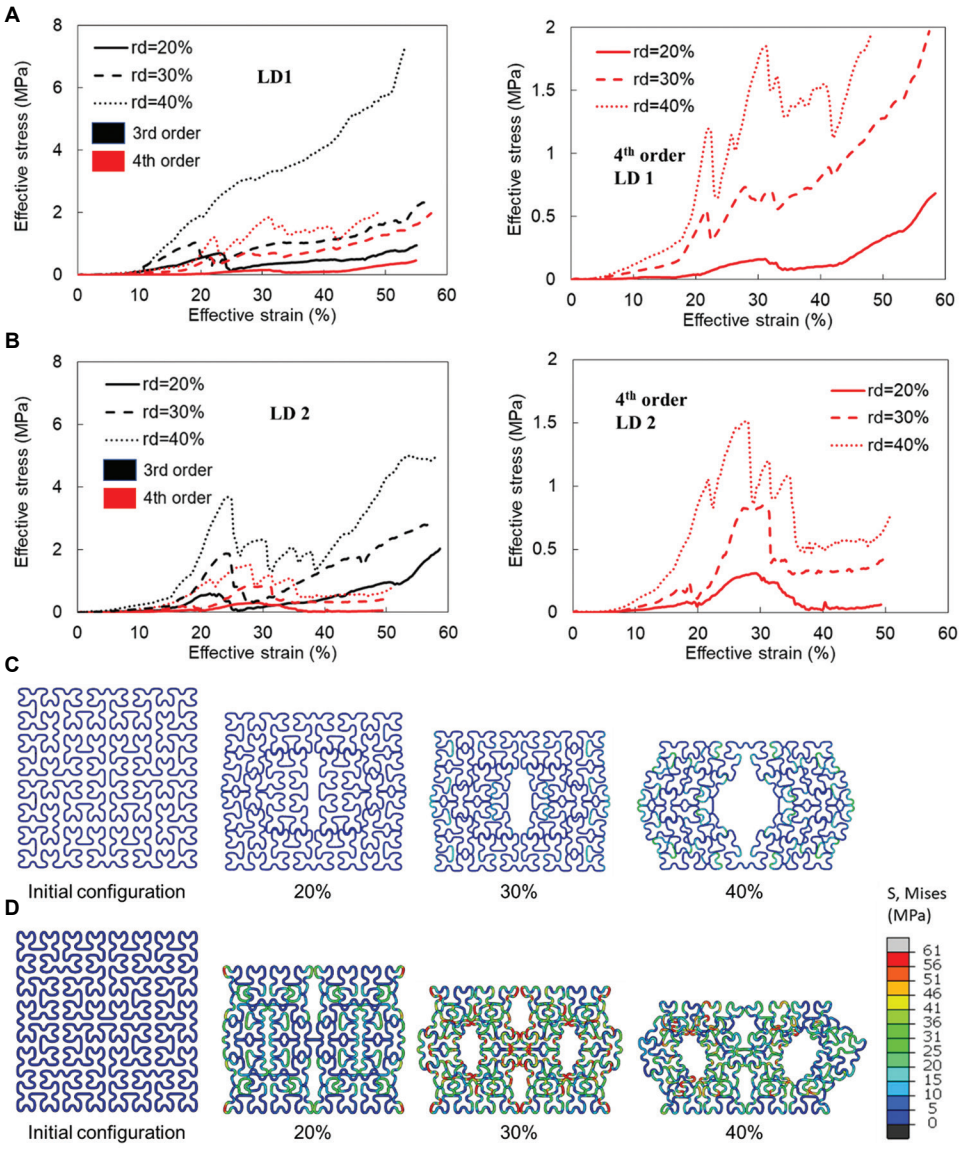

Figure 13. Comparison of effective stress-strain curves between the 3rd and 4th order structures (left panels), and magnified curves of the 4th order structures (right panels) obtained from FE models during quasi-static compression from (A) loading direction 1 (LD1) and (B) loading direction 2 (LD2). (C) Deformation of the 4th order structure with relative density (rd) of 20% under LD1. (D) Deformation of the 4th order structure with relative density of 40% under LD2. Shell elements are rendered with actual thickness.

strain and energy dissipation ratio demonstrated resilience in the 2nd order fractal-inspired thin-walled structure under cyclic loading from in-plane direction 1. This phenomenon was attributed to the less compliant behavior of the 2nd order structure when compared to the 3rd order structure.

Table 3. Specific energy absorption for the 4th order structures subjected to quasi-static compressive loadings

SEA (J/kg)	4th order structure	
	Loading direction 1	Loading direction 2
rd=20%	67.05	64.77
rd=30%	321.94	211.88
rd=40%	491.68	339.08

rd: relative density

3.5. Parametric study

A parametric study using FE simulation was conducted on 4th order structures with different relative densities to further explore the influences of fractal hierarchy and relative density on structural responses. To compare the responses of the 4th order structures with the 1st, 2nd, and 3rd order structures, the effective stress-strain curves of the 3rd order structures were used as references (Figure 13A and B). As revealed in Figure 13A and B (left panels), the 4th order structures yielded more compliant behaviors than the 3rd order structures at any given relative density in both LD1 and LD2. The increase by one fractal order led to quadruple complexity and meandering features in the cross-sectional configuration. The large number of curved segments gave rise to more snap-in instability and structural compliance, which were also manifested in more serrated stress-strain curves of the 4th order structures.

Figure 13A and B (right panels) shows clearer effective stress-strain curves of the 4th order structures, while Figure 13C and D displays the structural deformations of the 4th order structures under compression from LD1 (rd = 20%) and LD2 (rd = 30%), respectively. With the increase in relative density, the 4th order structure experienced higher stress in both in-plane directions due to its thicker wall-thickness. The drastic stress drops were created by the multiple simultaneous snap-ins (see 20% strain in Figure 13C and D). A plateau phase (Figure 13B [right panel]) in the effective stress-strain curves at a strain of 40% after the stress jump could be observed for all 4th order structures in LD2. This could be explained by the structural deformation in Figure 13D. After the 30% strain, both sides of the structure expanded outward in a transverse direction. The snap-ins along the side edges eventually unlocked and slid further outward, resulting in a long plateau phase. However, this was not observed in LD1 as only flat surface contacts, without snap-ins, occurred along the longitudinal edges (Figure 13C).

Table 3 summarizes the corresponding SEA for the 4th order structures under different loading directions. Consistent with the results obtained from the first three orders, SEA has a positive relationship with relative density for 4th order structures. However, the SEA in LD1 was more sensitive to increment in relative density compared to LD2. By comparing the values in Table 3 and Figure 11, it could be extrapolated that SEA decreases with the increase in fractal hierarchy after the 2nd order. The compliance feature and snap-in instability are more pronounced in higher orders, and the strength of the structures is sacrificed. Therefore, the energy absorption capacities are reduced for high order structures (higher than the 2nd order).

4. Conclusions

This paper presents a series of thin-walled structures inspired by Moore space-filling curves. Nine designs, featuring three hierarchies with three relative densities, that is, 20%, 30%, and 40%, were proposed and investigated. The FFF 3D printing technology was used to manufacture the samples with carbon fiber-reinforced nylon. Both quasi-static and loading-unloading compression tests were conducted to obtain and analyze the mechanical responses and energy absorption capacity of the proposed structures. Simulations were also performed to further elaborate the mechanical behaviors that were not observed from the experiment, that is, stress distribution. Herein, several conclusions were drawn.

(i) The space-filling feature of Moore curves offered great compliance to the thin-walled structures. All the fractal structures exhibited high level of flexibility, which could provide great potential for energy absorbing device with large strain endurance before failure. Fractal hierarchy was positively related to compliance, while relative density was the opposite.
(ii) The meandering pattern of Moore space-filling curves and the smooth geometry design enabled the snap-in of thin-walled structures. A certain degree of such instability reduced the stress within the structures, enhancing the energy absorption capacity. The 2nd order structures outperformed the 1st, 3rd, and 4th order structures in absorbing energy.
(iii) During quasi-static compression test, the SEA was relatively higher when subjected to LD2 than when subjected to LD1 due to the cross-sectional configuration and snap-in behavior.
(iv) In cyclic loading tests, the 2nd order structure exhibited better resilience. Smaller energy dissipation ratio and less residual strain indicated the promising ability of the 2nd order structure to resist deformation and damage from external loadings.

Overall, the proposed designs inspired by Moore space-filling curves in the present study open a new avenue for further research into the field of lightweight structures for energy absorption. The combination of thin-walled

structures with space-filling curve cross-sections can provide great compliance and snap-in instability. This fractal geometry is a promising candidate in the design of lightweight energy absorption structures.

Acknowledgments

The authors acknowledge the facilities and technical assistance from the Advanced Manufacturing Precinct and Microscopy and Microanalysis Facility and at RMIT University.

Funding

This research received no external funding.

Conflict of interest

The authors declare that they have no conflict of interest.

Author contributions

Conceptualization: Phuong Tran
Data curation: Changlang Wu
Formal analysis: Changlang Wu
Methodology: Phuong Tran
Supervision: Phuong Tran
Writing – original draft: Changlang Wu
Writing – review & editing: Vuong Nguyen-Van, Phuong Tran

All authors have read and agreed to the published version of the manuscript.

Ethics approval and consent to participate

Not applicable.

Consent for publication

Not applicable.

Availability of data

The authors confirm that the data supporting the findings of this study are available within the article.

References

1. Ma Y, Sugahara T, Yang Y, *et al*., 2015, A study on the energy absorption properties of carbon/aramid fiber filament winding composite tube. *Compos Struct*, 123: 301–311.
2. Nguyen-Van V, Liu J, Peng C, *et al*., 2022, Dynamic responses of bioinspired plastic-reinforced cementitious beams. *Cement Concrete Compos*, 133: 104682.
3. Nguyen-Van V, Wickramasinghe S, Ghazlan A, *et al*., 2020, Uniaxial and biaxial bioinspired interlocking composite panels subjected to dynamic loadings. *Thin Walled Struct*, 157: 107023.
4. Nguyen-Van V, Peng C, Hazell PJ, *et al*., 2023, Performance of meta concrete panels subjected to explosive load: Numerical investigations. In: *Structural Concrete*. United States: Wiley.
5. Sun G, Chen D, Zhu G, *et al*., 2022, Lightweight hybrid materials and structures for energy absorption: A state-of-the-art review and outlook. *Thin Walled Struct*, 172: 108760.
6. Mohsenizadeh M, Gasbarri F, Munther M, *et al*., 2018, Additively-manufactured lightweight Metamaterials for energy absorption. *Mater Des*, 139: 521–530.
7. Nguyen-Van V, Tran J, Peng C, *et al*., 2020, Bioinspired cellular cementitious structures for prefabricated construction: Hybrid design & performance evaluations. *Autom Constr*, 119: p. 103324.
8. Dang BL, Nguyen-Van V, Tran P, *et al*., 2022, Mechanical and hydrodynamic characteristics of emerged porous Gyroid breakwaters based on triply periodic minimal surfaces. *Ocean Eng*, 254: 111392.
9. Meredith J, Ebsworth R, Coles SR, *et al*., 2012, Natural fibre composite energy absorption structures. *Compos Sci Technol*, 72: 211–217.
10. Yang H, Lei H, Lu G, *et al*., 2020, Energy absorption and failure pattern of hybrid composite tubes under quasi-static axial compression. *Compos B Eng*, 198: 108217.
11. Tarlochan F, AlKhatib S, 2017, Energy Absorption Capabilities of Complex Thin Walled Structures. In: IOP Conference Series: Materials Science and Engineering. United Kingdom: IOP Publishing.
12. Nguyen-Van V, Choudhry NK, Panda B, *et al*., 2022, Performance of concrete beam reinforced with 3D printed Bioinspired primitive scaffold subjected to three-point bending. *Autom Constr*, 134: 104060.
13. Fu J, Liu Q, Kangmin L, *et al*., 2019, Design of bionic-bamboo thin-walled structures for energy absorption. *Thin Walled Struct*, 135: 400–413.
14. Nia AA, Hamedani JH, 2010, Hamedani, Comparative analysis of energy absorption and deformations of thin walled tubes with various section geometries. *Thin Walled Struct*, 48: 946–954.
15. Nia AA, Parsapour M, 2014, Comparative analysis of energy absorption capacity of simple and multi-cell thin-walled tubes with triangular, square, hexagonal and octagonal sections. *Thin Walled Struct*, 74: 155–165.
16. Wang S, Xia H, Liu YJ, 2022, Energy absorption characteristics of polygonal bio-inspired honeycomb column thin-walled structure under quasi-static uniaxial compression loading. *Biomimetics* (*Basel*), 7: 201.
17. Zhang XW, Su H, Yu TX, 2009, Energy absorption of an axially crushed square tube with a buckling initiator. *Int J Impact Eng*, 36: 402–417.
18. Xing BF, Dayong H, Sun YX, *et al*., 2015, Effects of hinges and deployment angle on the energy absorption characteristics

of a single cell in a deployable energy absorber. *Thin Walled Struct*, 94: 107–119.

19. Ali M, Ohioma E, Kraft F, *et al*., 2015, Theoretical, numerical, and experimental study of dynamic axial crushing of thin walled pentagon and cross-shape tubes. *Thin Walled Struct*, 94: 253–272.

20. Liu YJ, 2008, Crashworthiness design of multi-corner thin-walled columns. *Thin Walled Struct*, 46: 1329–1337.

21. Wang J, Liu Y, Wang K, *et al*., 2022, Progressive collapse behaviors and mechanisms of 3D printed thin-walled composite structures under multi-conditional loading. *Thin Walled Struct*, 171: 108810.

22. Vinayagar K, Kumar AS, 2017, Crashworthiness analysis of double section bi-tubular thin-walled structures. *Thin Walled Struct*, 112: 184–193.

23. Zhang Y, Wang J, Wang C, *et al*., 2018, Crashworthiness of bionic fractal hierarchical structures. *Mater Des*, 158: 147–159.

24. Wang J, Zhang Y, He N, *et al*., 2018, Crashworthiness behavior of Koch fractal structures. *Mater Des*, 144: 229–244.

25. Gao Q, Liao W, 2021, Energy absorption of thin walled tube filled with gradient auxetic structures-theory and simulation. *Int J Mech Sci*, 201: 106475.

26. Huang J, Zheng Z, Deng X, *et al*., 2022, Crashworthiness analysis of gradient fractal thin-walled structure. *Thin Walled Struct*, 181: 110102.

27. Hao P, Du J, 2018, Energy absorption characteristics of bio-inspired honeycomb column thin-walled structure under impact loading. *J Mech Behav Biomed Mater*, 79: 301–308.

28. Nguyen-Van V, Wu C, Vogel F, *et al*., 2021, Mechanical performance of fractal-like cementitious lightweight cellular structures: Numerical investigations. *Compos Struct*, 269: 114050.

29. Li Z, Shen L, Wei K, *et al*., 2021, Compressive behaviors of fractal-like honeycombs with different array configurations under low velocity impact loading. *Materials* (*Basel*), 163: 107759.

https://doi.org/10.3390/ma14175040

30. San Ha N, Pham TM, Chen W, *et al*., 2021, Crashworthiness analysis of bio-inspired fractal tree-like multi-cell circular tubes under axial crushing. *Thin Walled Struct*, 169: 108315.

https://doi.org/10.1016/j.tws.2021.108315

31. He Q, Wang Y, Gu H, *et al*., 2022, The dynamic behavior of fractal-like tubes with Sierpinski hierarchy under axial loading. *Eng Comput*, 38: 1285–1298.

32. Li K, Feng Y, Gao Y, *et al*., 2020, Crashworthiness optimization design of aluminum alloy thin-walled triangle column based on bioinspired strategy. *Materials*, 13: 666.

33. Chen W, Wierzbicki T, 2001, Relative merits of single-cell, multi-cell and foam-filled thin-walled structures in energy absorption. *Thin Walled Struct*, 39: 287–306.

34. Dadrasi A, Beynaghi M, Fooladpanjeh S, 2019, Crashworthiness of thin-walled square steel columns reinforced based on fractal geometries. *Trans Indian Inst Met*, 72: 215–225.

35. Fan ZG, Lu LX, Wang J, 2015, Effect of fatigue damage on energy absorption properties of honeycomb paperboard. *Shock Vib*, 2015: 1–7.

36. Van Vuong N, Quan MH, 2019, Fatigue analysis of jacket support structure for offshore wind turbines. *J Sci Technol Civil Eng*, 13: 46–59.

37. Zou Q, Zhou X, Wang R, *et al*., 2022, Load-carrying and energy-absorbing performance of honeycombs with different cross sections under cyclic loading. *Mat Today Commun*, 33: 104582.

38. Wu C, Do TT, Tran PJ, 2021, Mechanical properties of polyjet 3d-printed composites inspired by space-filling peano curves. *Polymers* (*Basel*), 13: 3516.

https://doi.org/10.3390/polym13203516

39. Wickramasinghe S, Do T, Tran P, 2022, Flexural behavior of 3D printed bio-inspired interlocking suture structures. *MSAM*, 1: 9.

40. Nguyen-Van V, Panda B, Zhang K, *et al*., 2021, Digital design computing and modelling for 3-D concrete printing. *Autom Constr*, 123: 103529.

41. Liu J, Nguyen-Van V, Panda B, *et al*., 2022, Additive manufacturing of sustainable construction materials and form-finding structures: A review on recent progresses. *3D Print Addit Manuf*, 2022. 9: 12–34.

42. Nguyen-Van V, Li S, Liu J, *et al*., 2022, Modelling of 3D concrete printing process: A perspective on material and structural simulations. *Addit Manuf*, 2022: 103333.

43. Peng C, Tran P, Mouritz A, 2022, Compression and buckling analysis of 3D printed carbon fibre-reinforced polymer cellular composite structures. *Compos Struct*, 300: 116167.

44. Zhang Y, Wei Y, Bai J, *et al*., 2022, A novel seawater and sea sand concrete-filled FRP-carbon steel composite tube column: Cyclic axial compression behaviour and modelling. *Compos Struct*, 252: 113531.

45. Alhyari O, Newaz G, 2021, Energy absorption in carbon fiber composites with holes under quasi-static loading. *C J Carbon Res*, 7: 16.

46. Zhang Y, Lu Z, Yang Z, *et al*., Resilient carbon fiber network materials under cyclic compression. *Carbon*, 155: 344–352.

47. Peng C, Tran P, Nguyen-Xuan H, *et al*., 2020, Mechanical performance and fatigue life prediction of lattice structures: Parametric computational approach. *Compos Struct*, 235: 111821.

48. Bunsell AR, 2018, Handbook of Properties of Textile and Technical Fibres. United Kingdom: Woodhead Publishing.

49. Wickramasinghe S, Do T, Tran P, 2020, FDM-based 3D printing of polymer and associated composite: A review on mechanical properties, defects and treatments. *Polymers*, 12: 1529.

50. Zhao B, Chen W, Hu J, *et al*., 2015, An innovative methodology for measurement of stress distribution of inflatable membrane structures. *Meas Sci Technol*, 27: 025002.

51. Alderson A, Alderson K, 2007, Auxetic Materials. Proceedings of the Institution of Mechanical Engineers Part G, *J Aerospace Eng*, 221: 565–575.